Nanocrystalline tungsten carbide (WC) synthesis/characterization and its possible application as a PEM fuel cell catalyst support

Zhu, Weimin; Ignaszak, Anna; Song, Chaojie; Baker, Ryan; Hui, Rob; Zhang, Jiujun; Nan, Feihong; Botton, Gianluigi; Ye, Siyu; Campbell, Stephen

Publisher's version / Version de l'éditeur:
https://doi.org/10.1016/j.electacta.2011.12.005
Electrochimica Acta, 61, pp. 198-206, 2011-12-09

Electrochimica Acta 61 (2012) 198–206

Contents lists available at SciVerse ScienceDirect

Electrochimica Acta

journal homepage: www.elsevier.com/locate/electacta

Nanocrystalline tungsten carbide (WC) synthesis/characterization and its possible application as a PEM fuel cell catalyst support

Weimin Zhu[a], Anna Ignaszak[a], Chaojie Song[a,*], Ryan Baker[a], Rob Hui[a], Jiujun Zhang[a], Feihong Nan[b], Gianluigi Botton[b], Siyu Ye[c], Stephen Campbell[d]

[a] Institute for Fuel Cell Innovation, National Research Council of Canada, 4250 Wesbrook Mall, Vancouver, BC, V6T 1W5 Canada
[b] Department of Materials Science and Engineering, McMaster University, 1280 Main Street West, Hamilton, ON, L8S 4L8 Canada
[c] Ballard Power Systems Inc., 9000 Glenlyon Parkway, Burnaby, BC, V5J 5J8 Canada
[d] AFCC Automotive Fuel Cell Cooperation, 9000 Glenlyon Parkway, Burnaby, BC, V5J 5J8 Canada

ARTICLE INFO

Article history:
Received 5 October 2011
Received in revised form 1 December 2011
Accepted 2 December 2011
Available online 9 December 2011

Keywords:
Tungsten carbide
Catalyst support
Oxygen reduction reaction
PEM fuel cells

ABSTRACT

Nanocrystalline tungsten carbide (WC) with a high surface area and containing minimal free carbon was synthesized via a polymer route. Its physical properties, including solubility in acid solution, electronic conductivity, and thermal stability, were thoroughly studied at two elevated temperatures: 95 °C and 200 °C. Compared to commercially available WC, this in-house synthesized WC showed lower solubility in acidic media at 200 °C, higher electronic conductivity (comparable to that of carbon black), as well as higher thermal stability. However, this material exhibited low electrochemical stability in acidic media when subjected to potential cycling at potentials larger than 0.7 V vs. RHE, due to the electrooxidation of WC. The major product of WC electrooxidation is WO_3, which was confirmed by X-ray photon spectroscopy measurements. Pt was uniformly deposited on the high surface area WC to form a 20 wt% of Pt supported catalyst for the oxygen reduction reaction (ORR). The ORR mass activity was then obtained using the rotating disk electrode technique.

1. Introduction

In the last several decades, proton exchange membrane (PEM) fuel cells, which have several advantages such as high power density, high energy density, and low/zero emission, have demonstrated their feasibility as practical energy conversion devices for many power-demanding fields including portable, automotive, and stationary applications. One of the major technical challenges, insufficient durability, is identified as a barrier hindering widespread commercialization of PEM fuel cells. It has been recognized that the degradation of fuel cell catalysts is the major cause for insufficient durability.

At the current state of technology, carbon-supported platinum (Pt)-based catalysts are the most practical for PEM fuel cell operation in terms of both catalyst activity and durability. Unfortunately, during fuel cell operation, Pt dissolution and carbon support oxidation/corrosion will occur, degrading the catalyst performance, and leading to low durability of the fuel cell. To address this challenge, one approach is to reduce carbon support corrosion by hybridizing the support materials or replacing some of the carbon content using non-carbon materials. With respect to this, intensive research has been done with a focus on the corrosion mechanism of carbon support and its prevention in the most recent years [1–3].

Currently, carbon blacks, such as Vulcan XC-72R and Ketjen black, have been used as the catalyst supports for PEM fuel cell catalysts because of their unique properties including sufficient electronic conductivity, high surface area, and suitable porous structure. However, under fuel cell operating conditions, carbon is prone to oxidation through the following reaction:

$$C + H_2O \rightarrow CO_2 + 4H^+ + 4e^-, \qquad E^o = 0.207\,\text{V vs.SHE} \tag{1}$$

At the fuel cell cathode, the normal operation potential (0.5–0.9 V vs. RHE) is more positive than the carbon oxidation potential. During the start-up/shutdown process, the potential can reach as high as 1.5 V vs. RHE (reversible hydrogen electrode), significantly higher than the carbon oxidation potential. These electrode potentials facilitate carbon oxidation through reaction (1). Furthermore, the presence of Pt and/or high temperature operation of the PEM fuel cell can accelerate carbon oxidation/corrosion. Obviously, this carbon oxidation/corrosion can result in the isolation of Pt catalyst particles and Pt catalyst agglomeration, degrading the fuel cell performance significantly [4]. Therefore, the

* Corresponding author. Tel.: +1 604 221 3000x5577; fax: +1 604 221 3001.
E-mail address: chaojie.song@nrc.gc.ca (C. Song).

0013-4686/$ – see front matter.
doi:10.1016/j.electacta.2011.12.005

development of high performance non-carbon support material, to replace carbon is imperative. This, however, turns out to be not an easy task, because a high performance catalyst support should meet all of the following requirements: high thermal stability, high electronic conductivity, low solubility in acidic media, high electrochemical stability, high surface area, as well as favourite interaction with the catalyst particles.

Among the non-carbon support candidates, tungsten carbide (WC) appears to be attractive. As a refractory metal carbide traditionally for erosion resistant coatings, WC has a high thermal stability and is chemically inert. The experimental results showed that, under ambient conditions, the oxidation of WC starts at around 600 °C [5], much higher than the operating temperature of PEM fuel cells. WC also exhibits good electronic conductivity, which makes it an excellent material for diffusion barrier layers in the semi-conductor industry. In addition, the Pt like catalytic behaviour of WC could result in a synergetic effect with the catalyst, leading to an increase in catalytic activity [6].

Tungsten carbide supported Pt catalysts have been synthesized and used for the oxygen reduction reaction (ORR) as well as methanol oxidation, and have demonstrated their synergetic catalytic effect. Meng and Shen [7] prepared a carbon-based nanocrystalline W_2C using the intermittent microwave heating (IMH) method, then mixed with Pt/C and IMH treated again to form a catalyst. Their results showed that the composite catalyst obtained could exhibit a higher ORR onset potential, higher specific activity, as well as better oxygen reduction selectivity in the presence of methanol than that of the Pt/C catalyst, demonstrating a synergetic effect between the tungsten carbide and Pt. Nie et al. [8] synthesized a Pt–WC–W_2C/C catalyst using an improved one-step IMH. The Pt–WC–W_2C/C catalyst showed an even better ORR activity than those Pt–W_2C/C composite catalysts. Wang et al. [9] prepared high surface area tungsten carbide microspheres (with mixed WC and W_2C phases) using a hydrothermal polymer method. The Pt/tungsten carbide micro-spheres catalyst with uniformly distributed Pt particles exhibited a better ORR activity than the Pt/C catalyst, which was attributed to the large electrochemical surface area and the Pt–tungsten carbide synergetic effect. Zhu et al. [10] observed an enhanced ORR catalytic activity for Pt on tungsten carbide-modified-carbon support. Modification of carbon with tungsten carbide could also improve the thermal stability of the support. Ganesan and Ham [11–13] synthesized high surface area tungsten carbide (W_2C) microspheres and WC supports using a carbon sphere template. The catalyst with Pt (7.5%) loading on the W_2C microsphere showed higher activity towards methanol electro-oxidation than the conventional 20% Pt–Ru/Vulcan catalyst [11–13]. This is possibly due to a co-catalytic effect between Pt and tungsten carbide: tungsten carbide activates methanol to form a methoxy intermediate, and Pt promotes the decomposition of the methoxy species [12].

The high thermal stability, high electronic conductivity, as well as the synergetic catalytic effect with the catalyst, make tungsten carbide promising as a PEM fuel cell catalyst support especially for high temperature operation. However, the electrochemical stability of WC might be an issue that could prevent WC from applications in PEM fuel cells. Controversial literature results were reported regarding the electrochemical stability of WC and WC supported catalysts. Mazza and Trassatti [14] used WC as an inert electrode, which demonstrated good chemical and electrochemical stability below the oxygen evolution potential. Chhina [15] found that WC supported Pt catalyst was electrochemically more stable than the carbon supported commercial catalyst HiSpec 4000™ (Pt/Vulcan XC-72R) when subjected to continuous CV scans at elevated temperature (80 °C). Voorhies [16] found that WC could be chemically oxidized in 1 M H_2SO_4 at room temperature, and electrochemically oxidized at medium to high anodic potential. Weigert et al. [17] observed a large anodic peak at 0.6–0.8 V on the cyclic voltammograms (CVs) of WC thin film, which was attributed to the WC oxidation, and WO_3 was indeed detected by XPS on the surface after the CV scans. Lee [18] also found that WC was not electrochemically stable. However, some metals additions could prevent or slow down the electrochemical oxidation of WC, possibly due to a synergetic effect. For example, the electrochemical oxidation of WC could be slowed down by alloying with Ta, and the WC thin film, on which a mono-layer of Pt was deposited, remained unchanged after CV measurements, while the one without Pt deposition was completely oxidized into WO_3.

The improved electrochemical performance of the tungsten carbide based Pt catalyst [7–13], and the controversial results [14–18] regarding the electrochemical stability of tungsten carbide motivated the authors to make a thorough investigation of the physical, chemical, and electrochemical properties of WC to evaluate its possibility as a PEM fuel cell catalyst support.

It is worthwhile to note that in the literature, a considerable amount of work was focused on tungsten carbide/carbon composite supports. Since carbon will be electrochemically oxidized, leading to fuel cell performance degradation, the existence of carbon in the support may not be desirable. In addition, the tungsten carbide reported in some papers is a mixed phase (W_2C and WC), which is not suitable for PEM fuel cell catalyst support application because W_2C is electrochemically and thermodynamically less stable than WC [19]. From the point view of fundamental understanding, a carbon-free, single-phase WC support is desired and is the focus of this paper.

In our high temperature (HT) PEM fuel cell approach, in order to overcome the challenge of carbon support corrosion in HT PEM fuel cells, we synthesized a single-phase WC support with high surface area, and investigated its electronic conductivity, chemical stability in acidic solution, as well as the electrochemical stability. For ORR activity, this WC material was used as the Pt catalyst support to form Pt/WC catalyst, and the corresponding ORR mass activity as well as the electrochemical stability were investigated.

2. Experimental

2.1. Synthesis of WC support and Pt/WC catalyst

Tungsten carbide (WC) supports were synthesized using a polymer precursor route modified based on Ganesan's procedure [7,8]. Typically, 4.73 g of ammonium metatungstate (AMT, Fluka) and 1.21 g of resorcinol (Sigma–Aldrich) were dissolved in 1.63 mL of formaldehyde (37% in H_2O, Sigma–Aldrich) and 19.8 mL of deionized water. The solution was then refluxed at 95 °C for 24 h forming an orange precipitate. The precipitate was washed and dried at room temperature, and then heat-treated in a tube furnace under a mixture of Ar (flow rate: 160 mL/min) and H_2 (flow rate: 60 mL/min) gas flow at 1000 °C for 2 h to form WC. Afterwards, the furnace was cooled down to 700 °C and kept for 2 h under a H_2 flow (flow rate: 115 mL/min) to remove the extra carbon. The synthesized WC is denoted as WC-SYN in this paper. For Pt deposition to form WC-supported catalyst (Pt/WC), an intermittent microwave heating (IMH) assisted polyol method was employed to deposit Pt onto the WC support. Typically, 90 mg WC support was dispersed in 20 mL ethylene glycol (EG), and the pH was adjusted to 8.0 with 0.2 M NaOH EG solution. This WC suspension was then sonicated for 1 h, followed by adding 46.6 mg of H_2PtCl_6 (dissolved in 3 mL EG) drop wise into the WC suspension. Afterwards, the catalyst precursor suspension was heated in a microwave oven (LBP 111RS, Ladd Research, USA) at 600 W for 60 s, and then intermittently for 6 times with 10 s of microwaving each time. The product was then filtered, washed, and dried.

2.2. Structure and morphology characterizations

The structure of these WC samples was characterized by X-ray diffraction (XRD) and the lattice pattern of the WC support was observed using high resolution transmission electron microscopy (HRTEM) together with electron diffraction. The inter-planar distance of the lattice was measured based on the lattice fringe. Scanning electron microscopy (SEM) and transmission electron microscopy (TEM) were employed to study the morphologies of the WC precursors, WC products, and Pt/WC catalysts.

The XRD measurements were carried out using a Bruker D-8 diffractometer with a step size of 0.02° and an exposure time of 0.1 s for each step. SEM observations were carried out on a Hitachi S3500N scanning electron microscope with an operating voltage of 20 kV. Samples for TEM characterization were directly supported on a copper mesh with a carbon micro-grid. TEM investigations at relative low magnification were performed using a Philips CM12 operated at 120 kV. HRTEM observations were carried out using a JEOL-2010F electron microscope at an accelerating voltage of 200 kV with a Field-Emission Gun (FEG). This instrument is equipped with a Gatan Imaging Filter (GIF) for energy-filtered imaging and an energy dispersive X-ray (EDX) detector for elemental analysis and mapping. Experimentally obtained electron diffraction patterns were compared to electron diffraction patterns simulated with the software program JEMS.

2.3. Solubility test

The solubility of commercially available (Alfa Aesar) and synthesized WC powders were tested in 1 M H_2SO_4 at 95 °C and 200 °C, respectively, according to the following procedures: for the solubility test at 95 °C, a flask containing 200 mg of WC powder and 50 mL of 1 M H_2SO_4 was put in an oil bath with constant stirring, kept at this temperature for 24 h. Afterwards, the suspension was filtered, and the filtered solution was sent for ICP/MS (inductively coupled plasma mass spectroscopy) to analyze for W, from which the solubility of WC was calculated. The leftover powder was washed, dried, and subjected to XRD characterization to look for any phase changes; for the solubility test at 200 °C, an in-house made chemically inert vessel with a pressure sealing system was used. 200 mg of WC powder sample and 50 mL of 1 M H_2SO_4 were put into this vessel, which was then filled with N_2 gas at a pressure of 200 psi. The high pressure (200 psi) kept inside the vessel can prevent H_2O from evaporating at 200 °C, so that the concentration of H_2SO_4 does not change during the test. The vessel was then heated in an oil bath at 200 °C for 2 h. After cooling and depressurization, the suspension was filtered, and the solution analyzed using ICP/MS where the leftover powder was then washed, dried, and subjected to XRD characterization.

2.4. Thermal stability test

The thermal stability test was carried out at 200 °C for 96 h. Typically, certain amount of sample was put in a Muffle Furnace, held at 200 °C in air for 96 h. Then the sample was cooled down to room temperature and sent for XRD characterization to observe any phase changes.

2.5. Conductivity measurement

An in-house made conductivity cell, which consists of an Ultem cylinder (inner diameter = 0.5 cm) to hold the sample and two Cu pistons as electrodes, was used for conductivity measurement. A small amount of WC powder was placed in the conductivity cell, and a load was applied on the upper piston to keep a pressure of 80 kPa. The whole set up was put in a Muffle furnace to control the temperature. A Tsuruga 3566 AC m-Ohm tester with a four-point setup was used to measure the conductivity at a constant frequency of 1 kHz. The electronic conductivity of WC was measured at 95 and 200 °C.

2.6. Other physical tests

For surface area analysis, a Beckman Coulter SA-3100 Surface Area Analyzer was employed to obtain N_2 adsorption/desorption isotherm, from which the BET surface area of the WC sample was calculated. For the determination of free carbon content in the synthesized WC samples, thermal gravity analysis (TGA) using a Perkin Elmer Paris 6 Thermal Gravity Analyzer was carried out on the WC samples from room temperature up to 730 °C in air. The X-ray photoelectron spectroscopy (XPS) of the as-synthesized WC powder and the one after 700 cyclic voltammogram scans (from 0.05 V to 1.2 V, see below), taken by a Leybold MAX-200 X-ray Photoelectron Spectrometer, was used to analyze the surface compositions of the samples.

2.7. Electrode preparation and electrochemical measurements

To prepare a catalyst (Pt/WC) or support (WC) ink, 19 mg catalyst or support was dispersed in 9.5 mL isopropanol and 0.5 mL de-ionized water, sonicated for 1 h to form a catalyst or support ink. 24 μL of catalyst or support ink was uniformly deposited on a glassy carbon electrode with a geometric area of 0.20 cm^2 (Glassy carbon electrode diameter: 5 mm, AFE7M050GC, Pine Research Instrument) to form a catalyst or support layer. Afterwards, 7.1 μL Nafion® solution (50:1 in methanol) was deposited on top to form the electrode coating layer.

The electrochemical measurements were carried out using a conventional three-electrode cell containing 0.1 M $HClO_4$ aqueous solution. For ORR measurement, this electrolyte solution was saturated with pure oxygen (bubbled by pure oxygen gas). For CV, this solution was bubbled with pure nitrogen gas to remove all dissolved oxygen. An RHE (reversible hydrogen electrode) was used as the reference electrode and a Pt wire as the counter electrode. The measurements were taken on a Solartron 1480 multi-potentiostat, controlled by Corrware software. For the electrochemical stability test, the electrode was immersed in 0.1 M deoxygenated (bubbling with N_2) $HClO_4$ solution at 30 °C, and the CV curves were recorded from 0.05 V to 1.2 V with a scan rate of 20 mV/s up to 1000 scans. From the CV curves, the electrochemical surface area was calculated from hydrogen adsorption/desorption peaks between 0.05 V and 0.4 V. For the ORR measurements, the voltammogram was recorded with a RDE (rotating disc electrode) in a 0.1 M O_2-saturated $HClO_4$ solution with a scan speed of 5 mV/s. An ASR rotator (Pine Instrument) was used to control the rotation rate.

For electrochemical active surface area (ECA) measurement, CO stripping method was used. The potential of the catalyst loaded electrode will be held at 0.05 V vs. RHE in 0.1 M $HClO_4$ with CO purging until saturation of CO adsorption is reached. The electrolyte solution is purged with N_2 for 30 min to remove un-adsorbed CO. Then the potential of the electrode will be scanned from 0 to 1.0 V vs. RHE at a scan rate of 20 mV/s. The ECA will be calculated from the charge of the CO oxidation peak according to Eq. (1′):

$$\mathrm{ECA} = \frac{Q_{\mathrm{CO\ adsorption}}}{0.42} \times 1000 \qquad (1')$$

where $Q_{\mathrm{COadsorption}}$ is the charge for CO oxidation in C, and 0.42 mC is the charge required to oxidize a monolayer of adsorbed CO on 1 cm^2 of Pt surface.

Table 1
Properties of WC samples.

	BET surface area (m^2/g)	Solubility (wt%)		Conductivity (S/cm)		Thermal stability
		95 °C	200 °C	95 °C	200 °C	
WC-Alfa	1.6	0.15	0.63	0.75	0.87	Stable up to 200 °C
WC-SYN	89	0.16	0.27	2.4	3.0	Stable up to 200 °C

3. Results and discussion

3.1. Properties of commercially available WC

As a preliminary assessment of WC as a catalyst support, the solubility, electronic conductivity, thermal stability, and electrochemical stability of commercially available WC (denoted as WC-Alfa hereafter) were investigated. The surface area of this catalyst is only 1.6 m^2/g.

As shown in Table 1, the solubility of WC-Alfa in 1 M H_2SO_4 at 95 and 200 °C is 0.15 wt% and 0.63 wt%, respectively. No phase change was observed on the XRD patterns after solubility tests (not shown here), indicating that this material has a low solubility and high chemical stability in 1 M H_2SO_4. The WC-Alfa was also found to be thermally stable at 200 °C. No phase change on the XRD pattern was observed (not shown here) after 96 h of heat treatment at 200 °C in air. The electronic conductivity of the WC-Alfa was found to increase with temperature from 0.75 S/cm at room temperature to 0.87 S/cm at 200 °C, which is in the same order as that of carbon black.

The cyclic voltammetry scans were conducted on WC-Alfa to evaluate its electrochemical stability. No oxidation/reduction peaks were observed within the potential range (0.05 V–1.2 V) up to 1000 CV scans (not shown here). This indicates the good electrochemical stability of WC-Alfa.

Based on the above preliminary assessment results on WC-Alfa, it seems that WC could be a suitable candidate as a PEM fuel cell catalyst support. However, the surface area of this WC-Alfa is fairly low (only 1.6 m^2/g). In order to obtain high ORR performance, a high surface area WC is desirable. We have thus synthesized a high purity nano-crystalline WC with high surface area.

3.2. Synthesis and purification of nano-crystalline WC

Fig. 1 shows the XRD pattern of the synthesized tungsten carbide (WC-SYN). It can be seen that a pure WC phase with only small amount of W metal (0.9 wt% based on the XRD peak area) was obtained, indicating that WC was successfully synthesized. Usually, WC synthesis involves high temperature, which results in low surface area products. However, a polymer synthesis procedure can reduce the synthesis temperature significantly. In this polymer synthesis procedure, a Bakelite type W–C complex precursor was formed as an intermediate phase [20]. This intermediate W–C complex phase could result in a W–C homogeneity at the molecular level, leading to significant decrease of the W–C alloying temperature compared to that for solid-state synthesis.

The WC phase obtained in this work is different from that reported in the literature. For example, Ganesen et al. [11,12] showed that the tungsten carbide product was dominated by W_2C. Normally, in WC synthesis, the reduction/carburization undergoes the following sequence: WO_3–WO_2–W–W_2C–WC [21,22]. Formation of tungsten carbide requires metallic W and active carbon that is produced on the W surface. The phase of the tungsten carbide product can be determined by two critical steps: the formation of active carbon C* on the W surface, and the diffusion of C* into the metallic W [22]. If the reduction of tungsten oxide into W is slow, the amount of C* formed will be low due to the lack of fresh W surface, and the diffusion of C into W will be fast, leading to the formation of W_2C. On the other hand, if the reduction of tungsten oxide into W is fast, there is enough W for the formation of C*, and the diffusion of C into W will become the limiting step. As a result, WC phase will be formed. In this work, in order to obtain pure WC phase, we increased the W precursor (ammonium metatungstate) content to create more W available for the formation of C*, and changed the gas environment from pure Ar to mixed gas flow of Ar and H_2 to speed up the reduction of tungsten oxide into W. These changes successfully show the formation of pure WC phase.

Fig. 2 shows the TGA result (in air) of the synthesized WC-SYN after 2 h of H_2 treatment. A weight gain starting from 400 °C can be observed, which is attributed to the oxidation of WC into WO_3. This weight gain reaches its maximum at around 600 °C, and then starts to decrease, which is due to burning of excess carbon. After 650 °C,

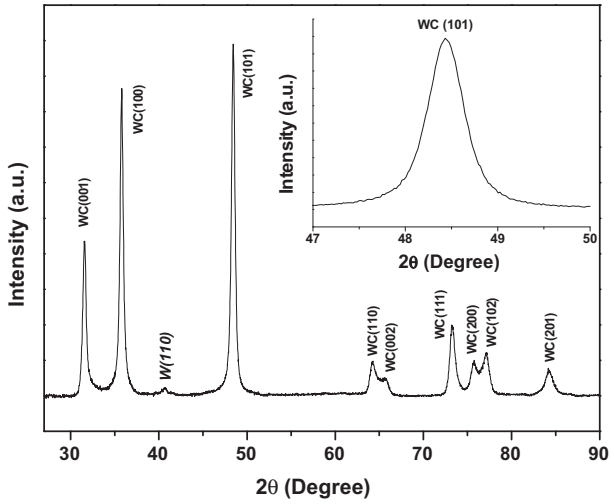

Fig. 1. XRD pattern of in-house synthesized WC sample (WC-SYN).

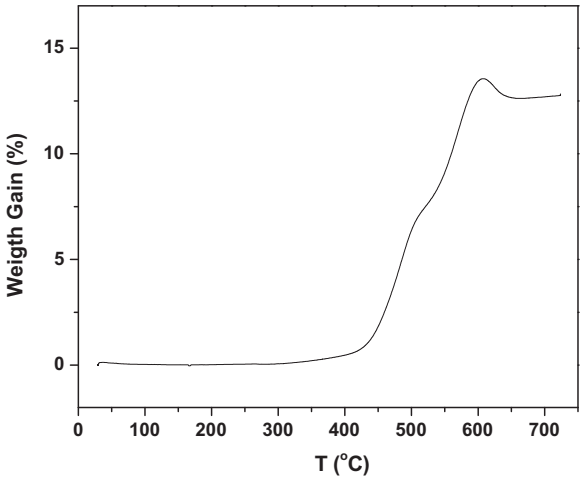

Fig. 2. Thermal gravity analysis (TGA) curve (in air) of WC-SYN.

the weight gain remains constant, indicating that the product has been completely oxidized. It is worthwhile to note that in this WC-SYN sample, some free carbon exists, which is not desirable.

In order to remove carbon (especially on the surface), the most common way is flushing the sample with H_2 at an elevated temperature via a methanization reaction. However, H_2 can also reduce WC into W depending on temperature, heat treatment time, as well as H_2 concentration. Since the methanization reaction has a lower Gibbs free energy than the WC reduction reaction, it might be possible, by optimizing these experimental parameters, to remove the excess carbon at a reasonable rate without significant formation of metallic W. Ribeiro et al. [23] reported that WC surface absorbed polymeric carbon, which could be removed after heat treatment in H_2 at 700 °C for 1.5 h. However after 2 h of heat treatment, metallic tungsten could be detected by XRD. The optimal condition of carbon removal by H_2 treatment depends on the particle size and surface properties of the WC product as well.

In this work, we treated the as-synthesized WC product at 700 °C for 2 h in a H_2 atmosphere. As shown in Fig. 2, the composition of the WC product can be found to be 94.2 wt% of WC, 0.9 wt% of W and 4.9 wt% of C, assuming that WC, W, and C are the only components. We also observed that extending H_2 treatment time did not lead to further reduction in C content, rather it increased W content. However, while decreasing H_2 treatment time, a higher C content was observed. Therefore, 2 h of H_2 treatment at 700 °C seemed to be the optimal time to remove the surface carbon on the WC product. It is believed that the remaining 4.9 wt% of carbon is inside the WC particles.

3.3. Properties of the in-house synthesized WC-SYN

The surface area, solubility, electronic conductivity, as well as the thermal stability of WC-SYN were tested in the same way as those for commercially available WC-Alfa. Table 1 summarizes the results. For comparison, the properties of WC-Alfa were also presented.

The surface area of WC-SYN was measured using N_2 adsorption/desorption isotherm and the obtained data was compared with that of WC-Alfa. From the isotherm curve (Fig. 3), a BET surface area of 89 m^2/g was obtained for WC-SYN, which is significantly higher than WC-Alfa that is only 1.6 m^2/g.

The solubility of WC-SYN at 200 °C is 0.27 wt%, lower than that of WC-Alfa. After solubility testing, a strong WO_3 peak could be seen on the recovered WC-SYN, while on the recovered WC-Alfa sample, there was no such WO_3 peak. This observation may suggest that the formation of insoluble WO_3 on the WC-SYN should be responsible for its lower solubility.

The conductivity of WC-SYN measured at 95 and 200 °C is listed in Table 1 together with those for WC-Alfa for comparison. It can be seen that the WC-SYN has a higher conductivity than WC-Alfa.

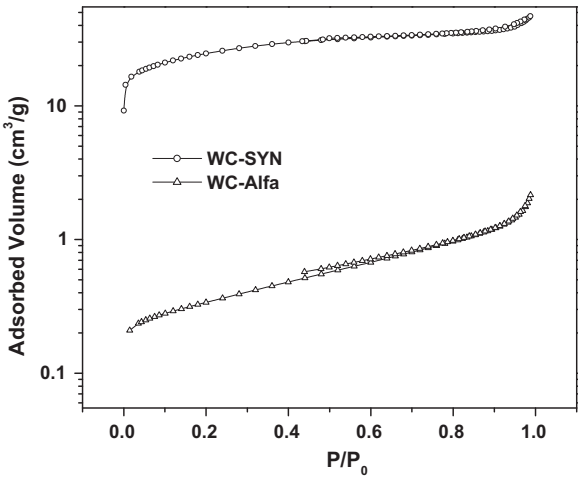

Fig. 3. N_2 adsorption/desorption isotherm curves for WC-Alfa and WC-SYN.

This higher conductivity of WC-SYN might be partially due to the existence of W metal, caused by post H_2 treatment.

Regarding the thermal stability of WC-SYN, no impure phase could be identified on the XRD pattern after the sample was heated in air at 200 °C for 96 h, indicating high thermal stability of WC-SYN.

3.4. WC-SYN morphologies and structure

Fig. 4 shows the SEM images of the WC-SYN precursor (a) and product after carbon removal (b). The WC-SYN precursor has a spherical morphology with sizes around 0.5–1.0 μm. However, after the synthetic process and heat treatment, these microspheres collapsed as seen in Fig. 4b and Fig. 5. This result is different from the literature [11], where microspheres morphology was retained in the final product. This collapse of the microsphere in the final WC product might be caused by lower carbon content in the precursor. Normally, carbon can act as skeleton for the microsphere. If the carbon content in the precursor is below a critical extent, the microsphere structure might collapse. The beneficial aspect is that this collapse can expose more surfaces for carbon removal, leading to a low C content.

Fig. 5 shows the TEM image of WC-SYN. Nano-particles with morphology of rice-like nanocrystals and whiskers can be clearly observed. The average particle size is about 35 nm according to the measurement over 200 particles (Fig. 6).

In order to further investigate the structure of WC-SYN, the HRTEM imaging together with the electron diffraction was carried out. As shown in Fig. 7, the WC-SYN exhibits a clear lattice fringes with well-defined single crystal-like electron diffraction pattern (Fig. 7c), indicating high crystallinity of WC-SYN particles. The

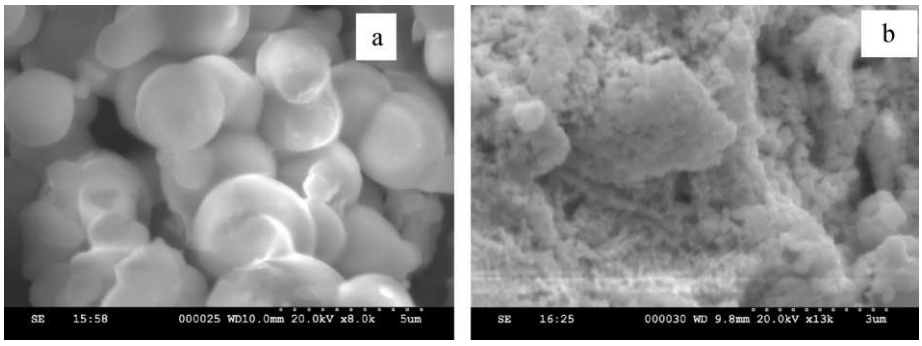

Fig. 4. SEM images of (a) WC-SYN precursor and (b) WC-SYN product.

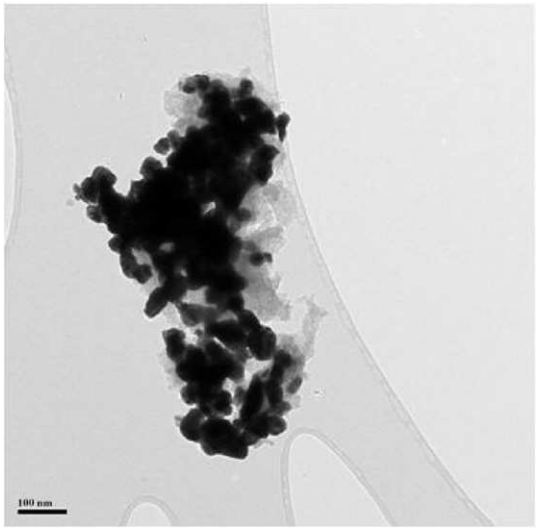

Fig. 5. TEM image of WC-SYN particles.

primary interplanar spacings on a low index zone axis are 2.57 and 2.92 Å, respectively (Fig. 7c), which are attributed to the (0 1 0) and (0 0 1) reflections and consistent with the hexagonal WC lattice (space group of P-6m2).

3.5. Pt/WC-SYN

To make a catalyst for the oxygen reduction reaction, Pt was deposited on the WC-SYN support by a polyol method. Fig. 8 shows the TEM image of 20 wt% Pt/WC catalyst. It can be seen that the Pt distribution on the WC support is fairly uniform, demonstrating the success in synthesizing Pt/WC catalyst. The average Pt particle size was found to be around 5 nm.

3.6. Electrochemical stability of WC-SYN and Pt/WC-SYN

In order to test the electrochemical stability of WC-SYN support and its supported Pt catalyst (Pt/WC-SYN), these materials were coated on the electrode individually, then tested in N_2-saturated 0.1 M $HClO_4$ solution at 30 °C using cyclic voltammetry. Fig. 9 shows the cyclic voltammograms (CVs) of WC-SYN. In the first cycle, a large anodic current was observed at potentials > 0.7 V vs. RHE. This

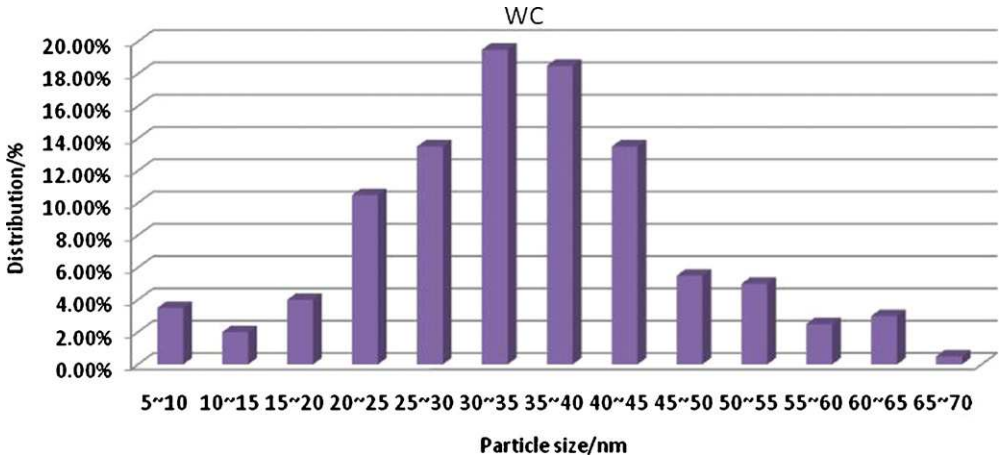

Fig. 6. Size distribution of WC-SYN particles.

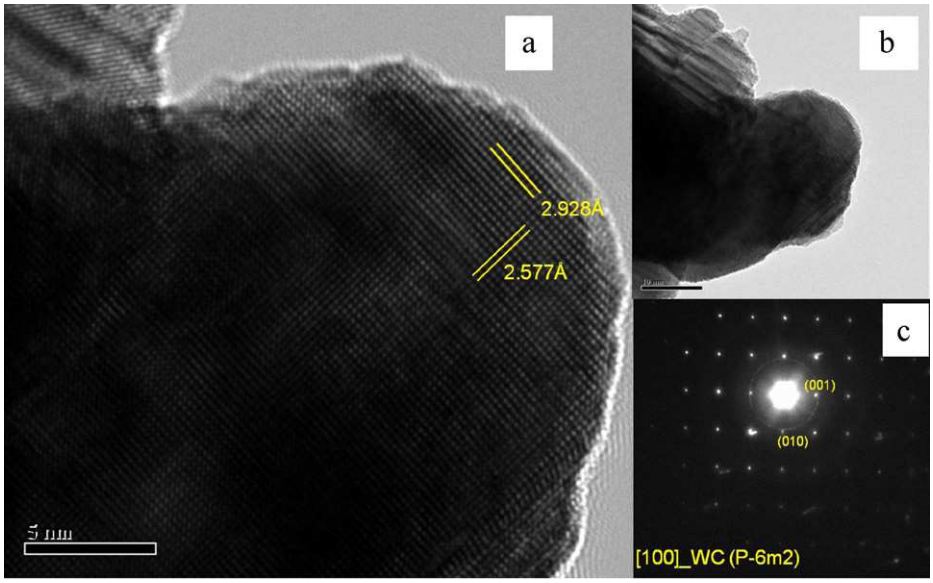

Fig. 7. (a) Enlarged HRTEM image of WC-SYN particle; (b) lower magnification view of a particle; and (c) the corresponding indexed selected area electron diffraction (SAED) pattern.

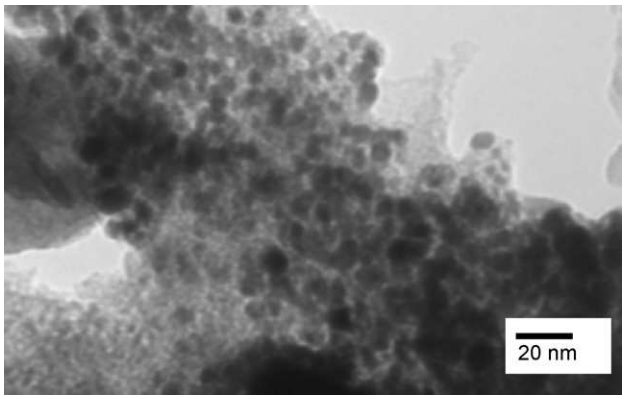

Fig. 8. TEM image of 20 wt% Pt/WC-SYN catalyst (average Pt particle size: 5 nm).

peak decreases as the CV scan proceeds, and finally disappears at the 100th CV scan. At the same time, redox peaks between 0.1 and 0.4 V vs. RHE on both anodic and cathodic scans become more and more prominent with increasing CV scan, and then slightly decrease after 100 CV cycles, especially for the cathodic peaks (Fig. 9b).

The large anodic current at >0.7 V vs. RHE should arise from the electrochemical oxidation of WC, as reported in the literature [17–19]. With the proceeding of CV scan, more and more WC was oxidized into WO_3, which covered the WC surface, resulting in gradually diminishing of this current.

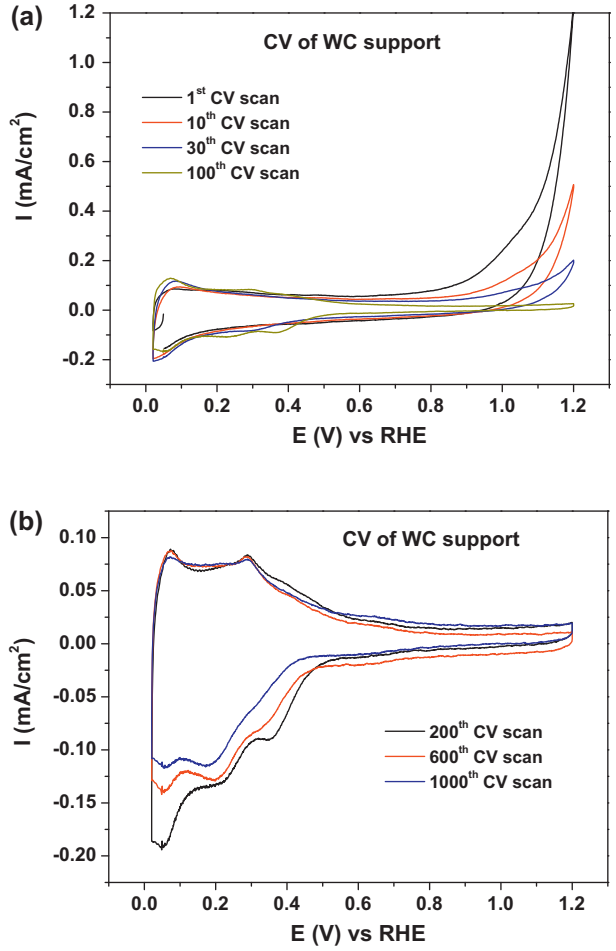

Fig. 9. Cyclic voltammograms of WC-SYN in a N_2-saturated 0.1 M $HClO_4$ solution. (a) First 100 scans, and (b) remaining 900 scan. Scan rate: 20 mV/s, temperature: 30 °C, and WC loading on the electrode: 48 μg/cm^2.

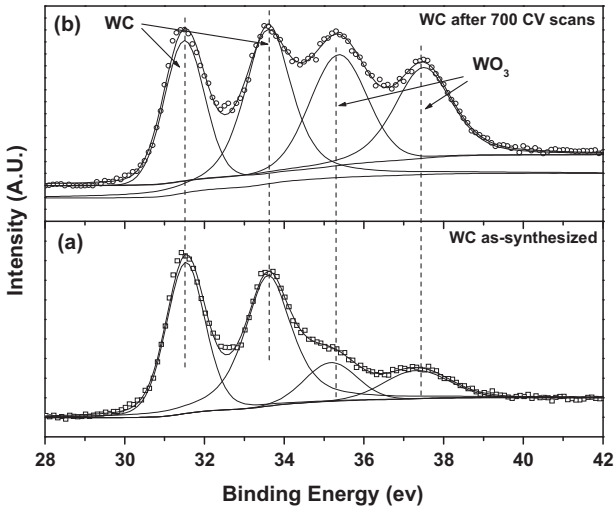

Fig. 10. XPS spectra of WC-SYN (a) before CV scan and (b) after 700 CV scans.

The peaks between 0.1 and 0.4 V vs. RHE could be attributed to the reversible redox process of WO_3/H_xWO_3 in acidic media [24–26]:

$$WO_3 + xH^+ + xe^- \leftrightarrow H_xWO_3 \quad (2)$$

At the cathodic scan, proton intercalates into WO_3, forming hydrogen tungsten bronze, resulting in cathodic peaks. At the anodic scans, when the potential increases to a certain value, H^+ will de-intercalate from the hydrogen tungsten bronze lattice, oxidizing H_xWO_3 back to WO_3, leading to anodic peaks. The intensities of these anodic and cathodic peaks were expected to increase with CV cycling because more WO_3 was produced. However, a decrease of the peak intensities was observed after 100 CV scans. This is likely due to the decrease in surface area caused by the WO_3 coverage [26].

In order to confirm the formation of WO_3 on the WC surface, XPS spectra were taken on WC-SYN before and after the CV scan, as shown in Fig. 10. For the as-synthesized WC, a W4f doublet with binding energies of 31.5 eV and 33.6 eV, can be observed, which corresponds to the WC phase. In addition, two peaks can also be found at higher binding energy (35.2 eV and 37.4 eV), corresponding to the $W4f_{7/2}$ and $W4f_{5/2}$ peaks of WO_3 phase (Fig. 11a). The presence of small amount of WO_3 on the surface of the as-synthesized

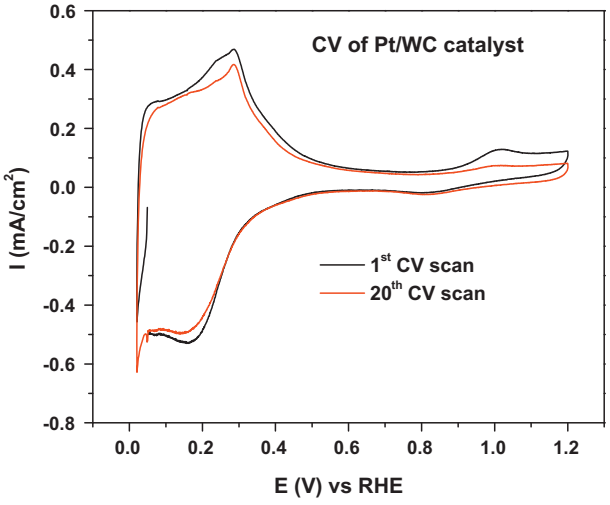

Fig. 11. Cyclic voltammograms of 20 wt% Pt/WC-SYN in N_2-saturated 0.1 M $HClO_4$ solution at 30 °C. Potential scan rate: 20 mV/s. Pt loading: 47.8 μg/cm^2.

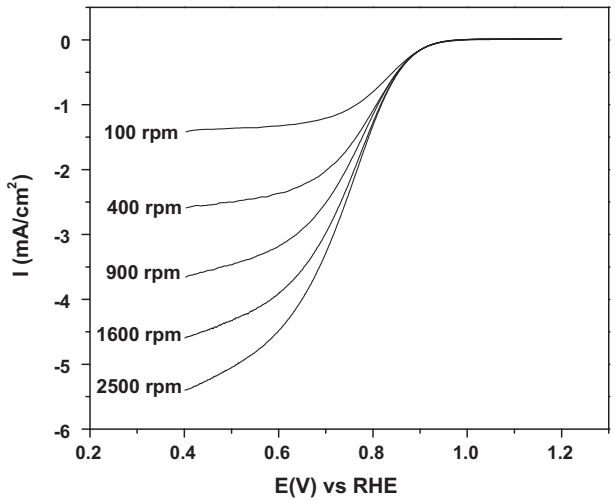

Fig. 12. Voltammetric curves at different rotation rates, recorded on a rotating disk electrode coated with 20 wt% Pt/WC-SYN catalyst in O_2-saturated 0.1 M $HClO_4$ solution at 30 °C. Scan rate: 5 mV/s. Pt loading: 47.8 μg/cm^2.

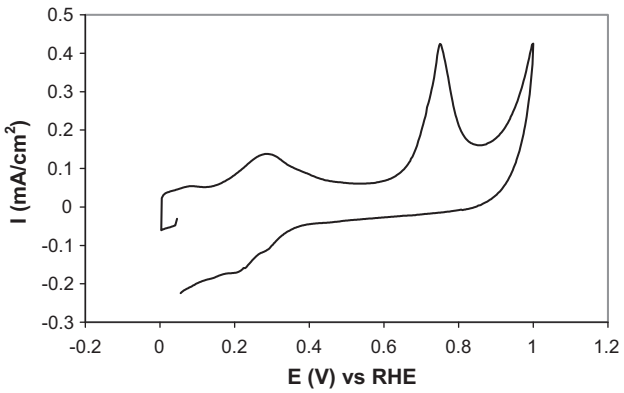

Fig. 13. The CO_{ads} stripping voltammogram on 20 wt% Pt/WC-SYN in 0.1 M $HClO_4$ at 30 °C. Scan rate: 20 mV/s, Pt loading: 48 μg/cm^2.

WC-SYN might be due to the oxidation of WC under ambient conditions [18]. After 700 CV scans, the intensity of the $W4f_{7/2}$ and $W4f_{5/2}$ peaks increased significantly (Fig. 11b), indicating an electrochemical oxidation of WC into WO_3. These XPS results confirm the conversion of WC into WO_3 on the surface of the WC-SYN as a result of CV cycling. It is in agreement with those reported by Weigert et al. [17] and Lee et al. [18].

CV cycling was also conducted on the Pt/WC-SYN catalyst to test the electrochemical stability of WC supported Pt catalyst. Fig. 11 shows the CV curve of the 20 wt% of Pt deposited on WC-SYN (20 wt% Pt/WC-SYN). Large hydrogen adsorption/desorption (from 0.05 V to 0.4 V) peaks, and disproportionally small Pt oxidation/reduction peaks were observed. The shape of the CV curve for the 20 wt% Pt/WC-SYN catalyst is very similar to that of the WC-SYN support (after 100 CV cycles), and the peak positions for the low potential region (0.1 V and 0.3 V) match well with that of H^+ intercalation/de-intercalation process in WO_3. Similar phenomena were also reported in the literature [27]. Therefore, this large hydrogen adsorption/desorption current is composed of two processes: H adsorption/desorption on Pt and hydrogen adsorption/desorption on WO_3.

Fig. 11 also shows that the intensity of the Pt oxidation peak decreases as the CV scan proceeds. This is possibly due to the electrochemical oxidation of WC-SYN. The formation of non-conductive WO_3 could isolate Pt particles deposited on it, leading to electrochemically inaccessible Pt particles. However, the large oxidation current at >0.7 V on bare WC-SYN (Fig. 9) was not observed on 20 wt% Pt/WC-SYN catalyst, indicating that the oxidation of WC in Pt/WC-SYN is not as severe as bare WC. This means that the presence of Pt on WC might stabilize WC or inhibit WC oxidation, consistent with the results reported in literature [17,18].

3.7. Electrocatalytic activity of Pt/WC-SYN towards oxygen reduction reaction

In order to evaluate the electrocatalytic activity toward ORR, the in-house synthesized 20 wt% Pt/WC-SYN catalyst was deposited on the electrode surface to form a catalyst layer, then put into an electrochemical cell for ORR measurements. Fig. 12 shows the CV curves recorded at various electrode rotation rates at 30 °C in O_2-saturated 0.1 M $HClO_4$ solution. An ORR mass activity of 3.3 mA/mg Pt was obtained from the 1600 rpm curve at 0.9 V vs. RHE after the limiting current correction. This value is significantly lower than that obtained with commercial Pt/C (110 mA/mg Pt [28]). In the literature, larger ORR mass activities were reported for Pt/WC catalysts such as 12 mA/mg Pt [7], and 24 mA/mg Pt [8] (converted from specific activity and Pt loading). However, in these cases, large amount of carbon was present in the catalyst either in the form of Pt/C and WC mixture [7] or Pt deposited on the WC + C composite support [8]. Obviously, part of the ORR mass activity comes from the Pt deposited on C. In addition, the Pt loading in Pt/WC is very high (from 50% to 100%) [8]. If the high density of WC is considered, such a high Pt loading could lead to the formation of a conducting Pt multilayer. Electrons involved in the HOR (hydrogen oxidation reaction) and ORR do not need to go through the support and the catalyst behaves like Pt black, resulting in high ORR performance.

In order to better understand what causes the low ORR mass activity, the ECA was measured by CO stripping, which is supposed to avoid WC support interference. Fig. 13 shows the CO stripping voltammogram. A clear CO oxidation peak between 0.6–0.8 V was observed. From Eq. (1′), the ECA was calculated to be 9 m^2/g Pt. For Pt with particle size of 5 nm, the theoretical external surface area should be 56 m^2/g Pt. This indicates that only 16% of the external surface is electrochemically active, which might be the main cause of the low ORR mass activity. The ECA can also be calculated by subtracting the H desorption peak on WC (Fig. 9) from that on Pt/WC (Fig. 11), which gives a value of 45 m^2/g. This value is close to the theoretical value and significantly larger than that obtained with CO stripping. Most possibly, the interaction between Pt and WC enhanced the H adsorption/desorption. However it did not affect O_2 adsorption and reduction on Pt, which is evidenced by the small Pt oxidation peak in Fig. 11.

Tafel diagram of the linear scan was plotted. The >0.9 V potential region was selected for the Tafel plot, because in that potential region, the ORR current is independent of the RDE rotation rate, as observed in Fig. 12, indicating a pure kinetic behaviour. Fig. 14 shows the Tafel plot of the Pt/WC-SYN catalyst. A linear relation between logarithm current density and potential is observed, which has a Tafel slope of 77 mV/dec, larger than the 60 mV/dec usually reported for Pt catalyzed ORR reaction at low overpotentials [29]. This larger Tafel slope indicates that this low mass activity is partly caused by the sluggish reaction kinetics.

The low Pt utilization and large Tafel slope obtained with the Pt/WC-SYN might be due to the contact resistance between the catalyst and the support if the support is oxidized. An insulating WO_3 layer may block the electron transfer between the catalyst and the support, isolating the Pt catalyst resulting in low Pt utilization.

In addition, there are many factors that can cause a low mass activity. For example, the non-uniform distribution and/or the agglomeration of the Pt catalyst on the support could decrease Pt utilization, unfavourable electronic interaction between the

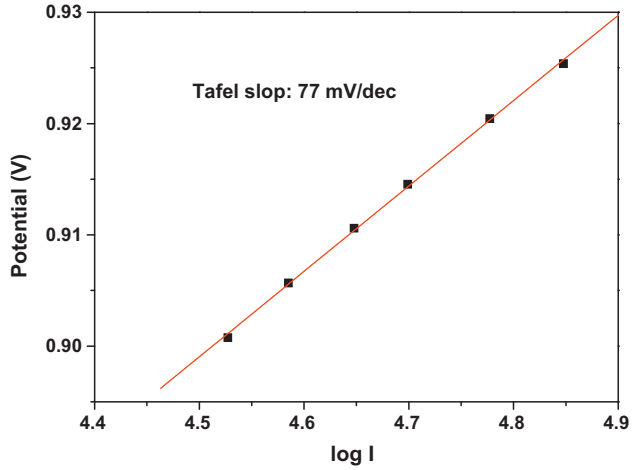

Fig. 14. Tafel plot of the ORR obtained with 20% Pt/WC-SYN catalyst in O_2-saturated, 0.1 M $HClO_4$, 30 °C. Scan rate of 5 mV/s, and RDE rotation rate: 1600 rpm.

catalyst and the support could also shift the onset potential of ORR to negative potential, and so on. These topics are definitely a continuing research area for future work.

4. Conclusions

Nano-crystalline WC with a surface area of 89 m^2/g and minimal carbon content was synthesized using a polymer route. The in-house synthesized WC (WC-SYN) has a high electronic conductivity, high thermal stability, as well as low solubility in acid when compared to commercially available WC-Alfa in the temperature range of 95 °C–200 °C. However, WC-SYN has a slightly lower electrochemical stability due to the electrooxidation into WO_3, which was confirmed by XPS measurements after the WC sample was potential cycling in the potential range of 0.0–1.2 V vs. RHE. This instability was attributed to its high surface area because the commercially available WC sample, which has a much lower surface area, was found to be electrochemically stable.

WC-SYN was tested as a Pt catalyst support. Uniformly distributed Pt particles were observed on WC-SYN. Electrochemical measurements showed that the presence of Pt did not catalyze WC oxidation. In contrary, it could slightly stabilize the WC-SYN support. However, the mass activity of ORR on a 20 wt% of Pt supported on WC-SYN was only 3.3 mA/mg Pt, significantly lower than commercial Pt supported on carbon. More work should be focused on improving the mass activity and the support stability of the WC supported Pt catalysts.

Acknowledgements

Financial support from National Research Council of Canada (NRC), Institute for Fuel Cell Innovation (IFCI) NRC, Ballard Power Systems, and AFCC (Automotive Fuel Cell Cooperation) through the Technology Development Program (TDP) is greatly appreciated. The authors would like to thank Mr. Ken Tsay at NRC-IFCI for the CO stripping measurement. Part of the electron microscopy was carried out at the Canadian Centre for Electron Microscopy, a facility supported by NSERC and McMaster University. GAB is grateful for a NSERC strategic grant for partially supporting FN and this work.

References

[1] W. Li, A.M. Lane, Electrochem. Commun. 11 (2009) 1187.
[2] A.A. Franco, M. Gerard, M. Guinard, B. Barthe, O. Lemaire, ECS Trans. 13 (2008) 35.
[3] H. Tang, Z. Qi, M. Ramani, J.F. Elter, J. Power Sources 158 (2006) 1306.
[4] H. Chhina, S. Campbell, O. Kesler, J. Power Sources 164 (2007) 431.
[5] C.A. Ribeiro, W.R. De Souza, M.S. Crespi, J.A. Gomez Neto, J. Therm. Anal. Calorim. 90 (2007) 801.
[6] R. Levy, M. Bourdat, Science 181 (1973) 547.
[7] H. Meng, P.K. Shen, J. Phys. Chem. B 109 (2005) 22705.
[8] M. Nie, P.K. Shen, M. Wu, Z. Wei, H. Meng, J. Power Sources 162 (2006) 173.
[9] Y. Wang, S.Q. Song, V. Maragou, P.K. Shen, P. Tsiakaras, Appl. Catal. B: Environ. 89 (2009) 223.
[10] Q. Zhu, S.H. Zhou, X.Q. Wang, S. Dai, J. Power Sources 193 (2009) 495.
[11] R. Ganesan, J. Lee, Angew. Chem. Int. Ed. 44 (2005) 6557.
[12] R. Ganesan, J. Ham, J. Lee, Electrochem. Commun. 9 (2007) 2576.
[13] J. Ham, K. Kim, H. Han, J. Lee, Catal. Today 132 (2008) 117.
[14] F. Mazza, T. Trassatti, J. Electrochem. Soc. 110 (1963) 847.
[15] H. Chhina, S. Campbell, O. Kesler, J. Power Sources 179 (2008) 50.
[16] J.D. Voorhies, J. Electrochem. Soc. 119 (1972) 219.
[17] E. Weigert, D. Esposito, J.G. Chen, J. Power Sources 193 (2009) 501.
[18] K. Lee, A. Ishihara, S. Mitsushima, N. Kamiya, K. Ota, Electrochim. Acta 49 (2004) 3479.
[19] M. Zellner, J.G. Chen, Catal. Today 99 (2005) 299.
[20] D.J. Ham, R. Ganesan, J.S. Lee, Int. J. Hydrogen Energy 33 (2008) 6865.
[21] E. Lessner, W.-D. Schubert, Tungsten: Properties, Chemistry, Technology of the Element, Alloys and Chemical Compounds, Springer, 1999.
[22] R. Koc, S.K. Kodambaka, J. Eur. Ceram. Soc. 20 (2000) 1859.
[23] F.H. Ribeiro, R.A. Dalla Betta, G.J. Guskey, M. Boubart, Chem. Mater. 3 (1991) 805.
[24] H. Binder, A. Kohling, W. Kuhn, W. Lindner, G. Sandstede, Nature 224 (1969) 1299.
[25] B.S. Hobbs, A.C.C. Tseung, Nature 222 (1969) 556.
[26] X. Cui, H. Zhang, X. Dong, H. Chen, L. Zhang, L. Guo, J. Shi, J. Mater. Chem. 18 (2008) 3575.
[27] D. Ham, Y. Kim, S. Han, J. Lee, Catal. Today 132 (2008) 117.
[28] H.A. Gasteiger, S.S. Kocha, B. Sompalli, F.T. Wagner, Appl. Catal. B: Environ. 56 (2005) 9.
[29] J.N. Soderberg, A.C. Co, A.H.C. Sirk, V.I. Birss, J. Phys. Chem. B 110 (2006) 10401.